Strong-field polarizability-enhanced dissociative ionization

Lun Yue,[1,*] Philipp Wustelt,[2,3] A. Max Sayler,[2,3] Florian Oppermann,[4] Manfred Lein,[4] Gerhard G. Paulus,[2,3] and Stefanie Gräfe[1,†]

[1]*Institute for Physical Chemistry and Abbe Center for Photonics, Friedrich-Schiller University, 07743 Jena, Germany*

[2]*Institute of Optics and Quantum Electronics, Friedrich-Schiller University, 07743 Jena, Germany*

[3]*Helmholtz Institute Jena, 07743 Jena, Germany*

[4]*Institute for Theoretical Physics, Leibniz University Hannover, 30167 Hannover, Germany*

(Received 13 July 2018; published 15 October 2018)

We investigate dissociative single and double ionization of HeH^+ induced by intense femtosecond laser pulses. By employing a semiclassical model with nuclear trajectories moving on field-dressed surfaces and ionization events treated as stochastical jumps, we identify a strong-field mechanism wherein the molecules dynamically align along the laser polarization axis and stretch towards a critical internuclear distance before dissociative ionization. As the tunnel-ionization rate is larger for larger internuclear distances and for aligned samples, ionization is enhanced. The strong dynamical rotation originates from the anisotropy of the internuclear distance-dependent polarizability tensor, which features a maximum at certain internuclear distances. Good qualitative agreement with our experimental observations is found. Finally, we investigate under which experimental conditions isotope effects of different isotopologues of HeH^+ can be observed.

DOI: 10.1103/PhysRevA.98.043418

I. INTRODUCTION

The ionization and dissociation of small molecules in intense laser fields is of fundamental interest and has captured the attention of physicists for many years [1–3]. When the ratio of the laser frequency to the peak electric field is sufficiently small, the ionization process can be considered as an electron tunneling through the instantaneous barrier formed by the field and the Coulomb potential of the system [4]. In molecules, such tunnel-ionization rates depend on the spatial separation between the nuclei [5–9], as well as the molecular orientation with respect to the laser polarization axis, where the ionization rate follows the shape of the highest-occupied molecular orbital [10–12]. In addition to these fixed-nuclei properties, the molecules will dynamically rotate and stretch in the field, potentially leading to fragmentation [8]. Here, we theoretically identify a fragmentation pathway that involves the combination of the aforementioned strong-field dynamics. Namely, due to the force resulting from the internuclear distance-dependent polarizability tensor, the molecule is simultaneously aligned and stretched towards a specific internuclear distance in the field-dressed ground state before being ionized. We denote it as polarizability-enhanced dissociative ionization (PEDI). We support our theoretical analysis with experimental data.

Polarizability effects have been explored extensively in strong-field physics, e.g., it has regularly appeared in the interpretation of strong-field ionization experiments [13,14], and the anisotropic polarizability is often exploited in molecular alignment experiments [15–17]. In dissociative ionization studies involving short laser pulses (tens of femtoseconds duration), often only the vibrational degrees of freedom are considered, while the rotational dynamics are disregarded. This is based on the intuition that the field-free rotational timescale of picoseconds is much greater than the vibrational timescale of femtoseconds and thus rotational motion can be safely neglected. However, as several works employing semiclassical methods [7,18,19] have shown, rotational dynamics are crucial for the understanding of the angular distribution of the final ion fragments. Even at lower intensities, where ionization is negligible and pure dissociation is the dominating fragmentation process, it was shown that molecular rotations play a role [20–24] for pulses as short as ∼5 fs.

For our studies, we choose to focus on the simplest stable polar molecule, HeH^+ [Fig. 1(d)]. Aside from HeH^+ being a reference system for polar molecules, the two lowest electronic states, $X^1\Sigma^+$ and $A^1\Sigma^+$ [see Fig. 1(a)], have a large energy separation of 13–39 eV in the Franck-Condon region and a small dipole coupling which goes to zero at large R. This highly limits the effect of the excited states and leads to the essential physics occurring in the field-dressed electronic ground state. Recent quantum calculations with vibrating HeH^+ also confirm the dominance of ionization from the ground state [25]. This is in stark contrast to homonuclear ions such as H_2^+, where the two lowest charge-resonance states [26] are energetically separated by a few IR photons at intermediate R, and degenerate and strongly coupled at large R. Indeed, most of the prominent breakup processes first discovered in H_2^+ depend on the efficient population of the first excited state. These processes include above-threshold dissociation [27–30], bond hardening and bond softening [31–34], electron localization [6,35–38], above-threshold Coulomb explosion [39], and charge-resonance

*lun_yue@msn.com

†s.graefe@uni-jena.de

 ©2018 American Physical Society

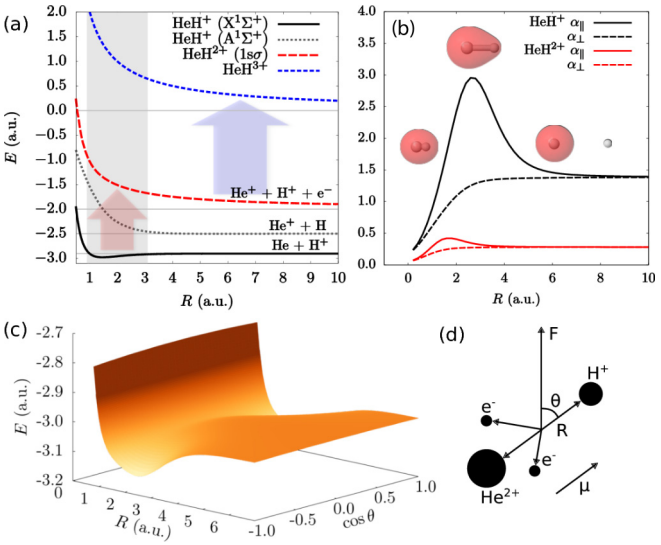

FIG. 1. (a) Field-free Born-Oppenheimer curves for HeH^+ and its daughter ions. The Franck-Condon region is indicated by the shading. (b) Polarizability tensors as a function of R. The electron densities (isosurface value 0.04) of HeH^+ $(X^1\Sigma^+)$ are plotted for $R = 1.0$, 2.6, and 6.0. (c) Cycle-averaged field-dressed potential for $F = 0.53$. (d) Sketch of HeH^+.

enhanced ionization [5]. Although PEDI should be present in H_2^+ as well as in other more complicated molecules, more prominent population and coupling of excited states may lead to other processes dominating, making an identification of PEDI difficult. It should be mentioned that the first excited state in HeH^+ has received attention in terms of the enhanced ionization (EI) phenomenon in polar molecules [9,40]: at a critical internuclear distance, due to the crossing of the two lowest Stark-shifted energy levels, enhanced population and ionization of the first excited state occurs. However, the EI description was based on a fixed-nuclei picture, and we find for a more realistic scenario, i.e., with moving nuclei and a molecule initially prepared close to the equilibrium R, the dominating effect is that ionization is enhanced due to the joined dynamics of rotation and stretching of the molecule.

II. THEORETICAL AND EXPERIMENTAL METHODS

In this article, strong-field dissociative single and double ionization (SI and DI) of HeH^+ is simulated employing a semiclassical approach with classical nuclear trajectories moving on field-dressed surfaces and ionization treated as stochastical jumps. Such an approach allows us to treat rotation, stretching, and single and double ionization while keeping the computational effort manageable to perform scans over an extensive laser-parameter space with inclusion of the initial rotational temperature, vibrational- and intensity-focal-volume-averaging effects. A full quantum treatment at the laser intensities considered in this work ($\lesssim 10^{16}$ W/cm^2) is computationally prohibitive.

In the HeH^+ sketch in Fig. 1(d), R denotes the internuclear distance and θ the angle between the field polarization and the molecular axes. The field-dressed energy surfaces read (atomic units are used unless stated otherwise)

$$E^{(s)}(R,\theta,t) = E_0^{(s)}(R) - \mu^{(s)}(R)F(t)\cos\theta - \tfrac{1}{2}F^2(t)\{\alpha_\perp^{(s)}(R) + [\alpha_\parallel^{(s)}(R) - \alpha_\perp^{(s)}(R)]\cos^2\theta\}, \quad (1)$$

with the superscript (s) indicating either the ground states of HeH^+ and HeH^{2+}, or the Coulomb potential of HeH^{3+} [Fig. 1(a)], F the electric field, $E_0^{(s)}$ the Born-Oppenheimer curves, $\mu^{(s)}$ the permanent dipole moments, and $\alpha_\perp^{(s)}$ ($\alpha_\parallel^{(s)}$) the molecular-frame perpendicular (parallel) components of the polarizability tensors (obtained on the CASSCF(15/2)/aug-cc-pVQZ [41] level of theory calculated with MOLCAS [42]). For HeH^+ $(X^1\Sigma^+)$, the anisotropic polarizability $\alpha_\parallel^{(s)} - \alpha_\perp^{(s)}$ exhibits a distinct maximum at $R_c = 2.6$ [Fig. 1(b)], which leads to distinct wells at R_c and $\cos\theta = \pm 1$ in the cycle-averaged field-dressed energy surface [Fig. 1(c)]. The peak in $\alpha_\parallel^{(s)}$ is understood in terms of the density isosurfaces in Fig. 1(b): For $R \to 0$ and $R \to \infty$, the electron cloud is spatially confined and resides almost completely on a single nucleus, resulting in small polarizabilities, while at intermediate R's the density is spatially extended, resulting in large polarizabilities. Recent quantum chemistry calculations on alkali dimers have also noticed the polarizability maximum and its possible implications for alignment experiments [43].

Each trajectory moves classically on the instantaneous field-dressed surface [Eq. (1)], with ionization treated as stochastical jumps [18,44]. For the pulses considered in this work, the Keldysh parameter is $\gamma < 1$, indicating the tunneling regime of strong-field ionization [4]. We employ the lowest-order many-electron weak-field asymptotic theory [45], where the ionization rate $\Gamma^{(s)}(F,\theta;R) = |G^{(s)}(\theta;R)|^2 W^{(s)}(F;R)$ is given by the *structure factor* $|G^{(s)}(\theta;R)|^2$ and the *field factor*

$$W^{(s)} = \frac{\kappa^{(s)}}{2}\left(\frac{4\kappa^{(s)2}}{F}\right)^{2Z^{(s)}/\kappa^{(s)}-1}\exp\left(-\frac{2\kappa^{(s)3}}{3F}\right), \quad (2)$$

with $\kappa^{(s)} = \sqrt{2I_P^{(s)}}$, $Z^{(s)}$ the nuclear charge seen by the outgoing electron asymptotically, and $I_P^{(s)}$ the ionization potentials. An additional empirical factor $\exp[-14Z^{(s)2}F/\kappa^{(s)5}]$ is applied to counteract the overestimation of the rates at large F [11]. The structure factors for $R = 1$–4 are obtained using the method in Ref. [46] and extrapolated to the values of the relevant atoms for $R \to \infty$. As shown in Fig. 2, the electron favorably tunnels from the hydrogen side, in agreement with earlier works [9,12,47]. The initial conditions of R and p_R are chosen randomly according to a Husimi distribution of a given vibrational state, and the molecules are chosen to be randomly oriented. The initial angular momenta are distributed according to a Boltzmann distribution to account for the high experimental rotational temperature in the ion source, $T = 3400 \pm 300$ K [48,49]. The laser wavelength is 800 nm and the pulse has a $\sin^2$ envelope with FWHM $\tau = 34$ fs. For each intensity and initial vibrational state, 10^3 trajectories are released. The results are averaged over the initial vibrational-state distribution [48], the laser beam focal volume [50], and the carrier-envelope phase, unless stated otherwise.

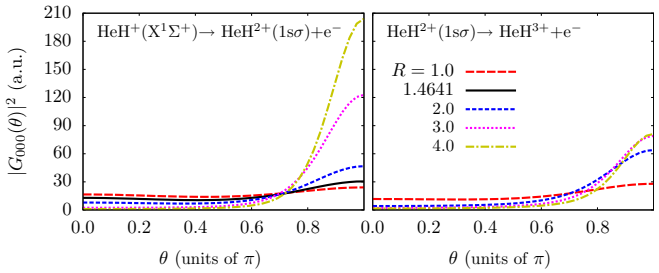

FIG. 2. Calculated structure factors $|G^{(s)}(\theta;R)|^2$ for single ionization of HeH^+ and HeH^{2+}, showing the orientation dependence of the ionization rates.

The experimental setup is identical to that described in Ref. [51]. Briefly, the HeH^+ ions are synthesized in a duoplasmatron ion source, accelerated to 10-keV kinetic energy, and focused towards the laser interaction region, where a tabletop Ti:sapphire laser system provides 800-nm pulses with peak intensities I of up to 10^{17} W/cm^2 and intensity FWHM duration $\tau \sim 34$ fs. Due to the low target density and the laser focal volume effect, much lower intensities are responsible for the ionization signal, and we therefore expect our simulation results with somewhat lower intensities ($\lesssim 10^{16}$ W/cm^2) to be adequately comparable to our experiment.

III. RESULTS AND DISCUSSIONS

Figure 3 shows the kinetic energy release (KER) and angular distributions of the nuclear fragments from SI and DI. Due to the high number of optical cycles, the directional ionization asymmetry for $\theta = 0$ and $\theta = \pi$ (Fig. 2) is averaged out, resulting in symmetric yields in the intervals $\cos\theta \in [0, 1]$ and $[-1, 0]$, of which we only consider the former.

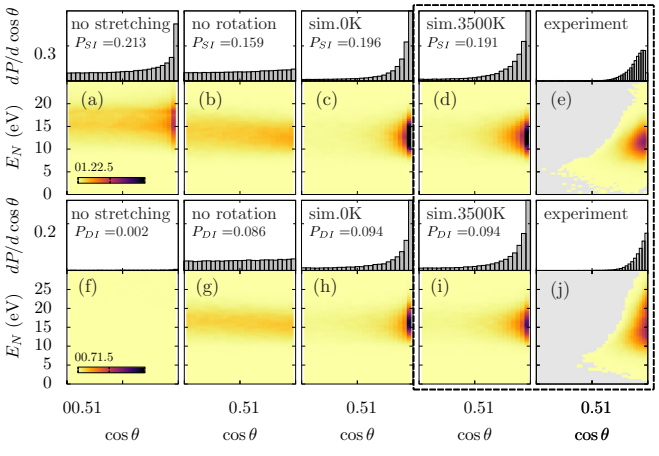

FIG. 3. KER- and orientation-dependent fragmentation yields from single (upper panels) and double dissociative ionization (lower panels) of HeH^+ for $\lambda = 800$ nm, $I = 9\times10^{15}$ W/cm^2, and $\tau = 34$ fs. (e), (j) Experimental results at laser peak intensity ($\sim 10^{17}$ W/cm^2), with the shaded area denoting absolute zero counts due to the experimental setup (see text). P_{SI} and P_{DI} denote the ionization probabilities. Results in the panels (a), (b), (f), (g) are with $T = 0$ K.

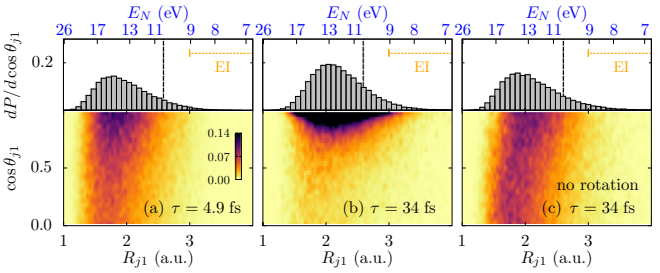

FIG. 4. Simulated distribution of R and $\cos\theta$ for the singly ionized molecules at the instant of ionization for $I = 9\times10^{15}$ W/cm^2 and $T = 0$ K: (a) $\tau = 4.9$ fs, (b) $\tau = 34$ fs, and (c) $\tau = 34$ fs with rotation disabled. The vertical dashed line indicates R_c. The horizontal line approximately traces the enhanced ionization region from [40] (not included in our simulations). The upper (blue) axis shows the kinetic energy by the reflection principle.

The SI experimental result in Fig. 3(e) shows that the fragments have KERs of 7–17 eV with the angular distribution aligned along the laser polarization direction ($\cos\theta = 1$). Due to the Faraday cup used in the experimental setup to block the nonfragmented HeH^+ beam, the yields at $\cos\theta \approx 1$ are not fully detected. Also, due to the finite size of the detector, the measurable range of $\cos\theta$ is limited, resulting in zero counts in the grayed region in Fig. 3(e). Our simulation results with $T = 3500$ K in Fig. 3(d) agree well with the experiment, with the fragments aligned along the laser polarization axis and having KER 7–18 eV, corresponding to ionization at $R \sim 1.5$–3.5 (see Fig. 4). Compared with Fig. 3(c), a nonzero temperature is seen to broaden the angular distribution. Three intertwined effects lead to the final aligned ion distribution: dynamic alignment during the laser pulse, geometric alignment [8,22] denoting the orientation-dependent ionization (Fig. 2), and postionization alignment [19]. By artificially disabling the molecular rotation in the simulations, we see in Fig. 3(b) that the angular distribution is quasiflat and cannot mimic the experimental results; thus geometric alignment plays a lesser role for the final ion angular distribution. Simulation results where we disabled the molecular stretching shown in Fig. 3(a) have too high KER (peaked at 17 eV) compared to the full result in Fig. 3(d), corresponding to ionization events occurring at smaller R's.

The measured DI yields in Fig. 3(j) are also aligned, with KER 8–25 eV, corresponding to the second ionization event occurring between $R \sim 5$–25 [51]. The simulation with $T = 3500$ K in Fig. 3(i) agrees with these observations. The angular distributions for SI and DI are similar, because after a molecule is singly ionized, it will dissociate and its moment of inertia MR^2 (M the reduced mass) increases, effectively freezing θ before DI. For both SI and DI, the ionization probabilities $P_{SI} = 0.192$ [Fig. 3(d)] and $P_{DI} = 0.071$ [Fig. 3(i)] are larger when the molecules are allowed to stretch and rotate, indicating increased ionization due to dynamical alignment and stretching towards $R = R_c$.

We estimate the rotational timescale as the time it takes a trajectory to reach from half of the well depth in Fig. 1(c) to the potential minima, i.e., $\tau_{\rm rot} = \sqrt{M}h(R)/F$, with $h(R) \approx 2.62R/\sqrt{\alpha_\parallel - \alpha_\perp}$. At R_c, with $M_{\rm HeH^+} = 1469$ and $F = 0.37$, we have $\tau_{\rm rot} = 12.8$ fs, which is comparable to the field-free

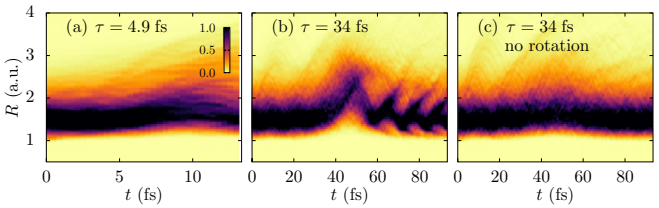

FIG. 5. Simulated time evolution of the nuclear densities for the artificial case with ionization turned off, for $I = 5\times10^{15}$ W/cm^2 and $T = 0$ K: (a) $\tau = 4.9$ fs, (b) $\tau = 34$ fs, and (c) $\tau = 34$ fs with rotation disabled. The results are vibrational averaged, but not intensity-focal-volume averaged.

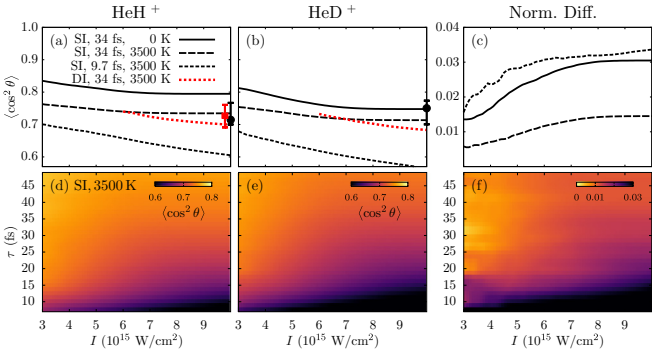

FIG. 6. Alignment parameter $\langle\cos^2\theta\rangle$ for (a), (d) HeH$^+$, (b), (e) HeD$^+$, and (c), (f) their normalized difference. In (a), (b), the fitted experimental results at peak intensity, 800 nm and 34 fs for SI and DI, are given by the (black) circle and (red) square, with the bars denoting the uncertainty in the fit (see text).

vibrational period $\tau_{\rm vib} = 11.5$ fs and 37 times shorter than that of the field-free rotational period of 478 fs. Dynamical rotation is expected to be prominent when the rotational timescale $\tau_{\rm rot}$ is comparable to or shorter than the pulse duration τ, which is the case for $\tau = 34$ fs used in the experiment.

Figure 4 shows the (R_{j_1}, θ_{j_1}) distribution of the singly ionized molecules at the instant of ionization. For the results in Fig. 4(c) with rotation artificially disabled, ionization occurs over a broad range of $\cos\theta_{j_1}$. With increasing $\cos\theta_{j_1}$, the ionizations are seen to be shifted towards larger R_{j_1}, e.g., we have $R_{j_1} \approx 1.8$ for $\cos\theta_{j_1} = 0$, and $R_{j_1} \approx 2.2$ for $\cos\theta_{j_1} = 1$. Also, more ionization events occur for the aligned molecules ($\cos\theta \approx 1$). The reason is clear: without rotation, the aligned molecules need to stretch towards larger R [see Fig. 1(c)], where the lower I_p and the favorable structure factor in Fig. 2 leads to more ionization. The projected R_{j1} distribution in the upper panel of Fig. 4(c) peaks at $R_{j_1} \approx 1.9$, corresponding to $E_N \approx 14$ eV by reflection. This is in disagreement with the experimental KER maximum in Fig. 3(e) at $E_N \approx 11$ eV. For the simulation results in Fig. 4(b) where rotational motion is included, most molecules ionize after they are dynamically aligned, with the projected R_{j_1} distribution peaked at $R \approx 2.1$, corresponding to a reflected KER $E_N \approx 12.5$ eV, in better agreement with the experiment. For the short pulse $\tau = 4.9$ fs $\lesssim \tau_{\rm rot}$ in Fig. 4(a), the molecules do not have much time to rotate and stretch, resulting in smaller R_{j_1}'s and thus much higher KERs. We have not taken the EI effect [9,40,47] into account in our ionization rates, which will take place at $R \gtrsim 3$ (horizontal dashed lines in Fig. 4). Since most ionization events occur before this region, we expect its effect to be small.

To understand more in detail the bound-state dynamics before ionization, we consider the artificial case with ionization switched off. The time evolution of the bound nuclear densities is shown in Fig. 5. Since the low-intensity regions in the focal volume dominate, we consider a single intensity without performing the focal-volume averaging. For the short pulse in Fig. 5(a), $\tau < \tau_{\rm rot} \approx \tau_{\rm vib}$, and the trajectories do not have time to rotate and vibrate, resulting in a minimal change of the density during the pulse. This is different for the long pulse shown in Fig. 5(b), where the molecules have time to align and stretch towards R_c, and at the field maximum $t = 46.7$ fs a substantial part of the density has reached $R \in [2, 3]$. During the second half of the pulse, the already aligned molecules contract back towards the equilibrium R_0, with density oscillations due to the vibrational motion distinctly observed in Fig. 5(b). When the molecule is not allowed to rotate [Fig. 5(c)], similar to the case of a short pulse, the stretching of the nuclei follows the dressed potential, but only molecules initially aligned along the laser polarization direction ($\cos\theta = 1$) stretch towards R_c.

The degree of alignment can be characterized by the alignment parameter $\langle\cos^2\theta\rangle$ (equal to 1 for completely aligned samples and $\frac{1}{3}$ for randomly oriented samples) and is given as a function of I for the fragmented HeH$^+$ in Fig. 6(a). For SI, higher temperature and shorter pulses result in broader angular distributions. With increasing intensities, the detected fragments are seen to be less aligned, despite the rotational timescale $\tau_{\rm rot} \propto 1/F$ being shorter. This is indeed a characteristic of dynamical rotation: with increasing I, ionization will occur earlier during the pulse, leaving the molecule with less time to rotate [8]. The experimental values for $\langle\cos^2\theta\rangle$ are shown in Fig. 6(a) as a circle and square for SI and DI, respectively. To avoid inaccuracies resulting from the properties of the experimental setup, we consider only the counts in the interval $E_N \in [0, E_{\rm max}]$ in Figs. 3(e) and 3(j), with $E_{\rm max} = 7$ eV, and fitted the missing yields at $\cos\theta \approx 1$ with a function $f(\cos\theta) = a\cos^2\theta + b\cos^c\theta$. The bars belonging to the data points are for the extremal values of $\langle\cos^2\theta\rangle$ for $E_{\rm max} \in [4, 9]$ eV and are seen to be consistent with the simulation results.

Since $\tau_{\rm rot} \propto \sqrt{M}$, the dynamical rotation is influenced by the specific isotope. Indeed, recently the isotope effect in tunneling ionization of molecules has attracted considerable attention [52,53]. We investigate whether an isotope effect can be observed in the ion angular distributions of HeH$^+$ and HeD$^+$. Figure 6(b) presents the simulated and experimental results for HeD$^+$. With the employed experimental laser parameters, however, this isotope effect cannot be conclusively resolved. To experimentally identify this would require shorter pulses, as depicted in Fig. 6(c), showing the normalized difference between the curves in Figs. 6(a) and 6(b), $S \equiv (\langle\cos^2\theta\rangle_{\rm HeH^+} - \langle\cos^2\theta\rangle_{\rm HeD^+})/(\langle\cos^2\theta\rangle_{\rm HeH^+} + \langle\cos^2\theta\rangle_{\rm HeD^+})$. For the 34-fs, 3500-K case, $S < 0.014$, while for the 9.7-fs pulse, S has more than doubled to 0.033. In Figs. 6(d)–6(f) we show $\langle\cos^2\theta\rangle$ for HeH$^+$, HeD$^+$ and their relative differences over an extensive pulse regime. It is seen

that the isotope effect for dynamical rotation is pronounced for pulse durations of less than 10 fs, potentially allowing for an experimental detection.

IV. CONCLUSION

In conclusion, we have identified polarizability-enhanced dissociative ionization, a strong-field molecular breakup pathway where the molecules dynamically align and stretch towards a specific internuclear distance before ionization, with geometric alignment playing a lesser role. For our studies, we have focused on the fundamental polar molecules HeH^+ and HeD^+, and we believe that the effect is general, though more pronounced for polar diatomics. Indeed, the maximum in the anisotropy polarizability is present in all diatomics, except for odd-charged molecular ions where the parallel polarizability will monotonically increase with R [26].

ACKNOWLEDGMENTS

The authors acknowledge support from the German Research Foundation (DFG-SPP-1840 "Quantum Dynamics in Tailored Intense Fields"). L.Y. thanks Johannes Steinmetzer for aiding in the calculation of the molecular polarizabilities.

[1] A. Giusti-Suzor, F. H. Mies, L. F. DiMauro, E. Charron, and B. Yang, Dynamics of H_2^+ in intense laser fields, J. Phys. B **28**, 309 (1995).

[2] J. H. Posthumus, The dynamics of small molecules in intense laser fields, Rep. Prog. Phys. **67**, 623 (2004).

[3] H. Ibrahim, C. Lefebvre, A. D. Bandrauk, A. Staudte, and F. Légaré, H_2: the benchmark molecule for ultrafast science and technologies, J. Phys. B **51**, 042002 (2018).

[4] L. V. Keldysh, Ionization in the field of a strong electromagnetic wave, Zh. Eksp. Teor. Fiz. **47**, 1945 (1964) [Sov. Phys. JETP **20**, 1307 (1965)].

[5] T. Zuo and A. D. Bandrauk, Charge-resonance-enhanced ionization of diatomic molecular ions by intense lasers, Phys. Rev. A **52**, R2511 (1995).

[6] T. Seideman, M. Y. Ivanov, and P. B. Corkum, Role of Electron Localization in Intense-Field Molecular Ionization, Phys. Rev. Lett. **75**, 2819 (1995).

[7] M. Plummer and J. F. McCann, Field-ionization rates of the hydrogen molecular ion, J. Phys. B **29**, 4625 (1996).

[8] J. H. Posthumus, J. Plumridge, M. K. Thomas, K. Codling, L. J. Frasinski, A. J. Langley, and P. F. Taday, Dynamic and geometric laser-induced alignment of molecules in intense laser fields, J. Phys. B **31**, L553 (1998).

[9] G. L. Kamta and A. D. Bandrauk, Phase Dependence of Enhanced Ionization in Asymmetric Molecules, Phys. Rev. Lett. **94**, 203003 (2005).

[10] A. S. Alnaser, S. Voss, X. M. Tong, C. M. Maharjan, P. Ranitovic, B. Ulrich, T. Osipov, B. Shan, Z. Chang, and C. L. Cocke, Effects of Molecular Structure on Ion Disintegration Patterns in Ionization of O_2 and N_2 by Short Laser Pulses, Phys. Rev. Lett. **93**, 113003 (2004).

[11] X. M. Tong and C. D. Lin, Empirical formula for static field ionization rates of atoms and molecules by lasers in the barrier-suppression regime, J. Phys. B **38**, 2593 (2005).

[12] O. I. Tolstikhin, T. Morishita, and L. B. Madsen, Theory of tunneling ionization of molecules: Weak-field asymptotics including dipole effects, Phys. Rev. A **84**, 053423 (2011).

[13] L. Holmegaard, J. L. Hansen, L. Kalhøj, S. L. Kragh, H. Stapelfeldt, F. Filsinger, J. Kupper, G. Meijer, D. Dimitrovski, M. Abu-samha, C. P. J. Martiny, and L. B. Madsen, Photoelectron angular distributions from strong-field ionization of oriented molecules, Nat. Phys. **6**, 428 (2010).

[14] A. N. Pfeiffer, C. Cirelli, M. Smolarski, D. Dimitrovski, M. Abu-samha, L. B. Madsen, and U. Keller, Attoclock reveals natural coordinates of the laser-induced tunneling current flow in atoms, Nat. Phys. **8**, 76 (2011).

[15] H. Stapelfeldt and T. Seideman, *Colloquium*: Aligning molecules with strong laser pulses, Rev. Mod. Phys. **75**, 543 (2003).

[16] R. Damari, S. Kallush, and S. Fleischer, Rotational Control of Asymmetric Molecules: Dipole- Versus Polarizability-Driven Rotational Dynamics, Phys. Rev. Lett. **117**, 103001 (2016).

[17] K. Lin, P. Lu, J. Ma, X. Gong, Q. Song, Q. Ji, W. Zhang, H. Zeng, J. Wu, G. Karras, G. Siour, J.-M. Hartmann, O. Faucher, E. Gershnabel, Y. Prior, and I. S. Averbukh, Echoes in Space and Time, Phys. Rev. X **6**, 041056 (2016).

[18] P. Dietrich, D. T. Strickland, M. Laberge, and P. B. Corkum, Molecular reorientation during dissociative multiphoton ionization, Phys. Rev. A **47**, 2305 (1993).

[19] X. M. Tong, Z. X. Zhao, A. S. Alnaser, S. Voss, C. L. Cocke, and C. D. Lin, Post ionization alignment of the fragmentation of molecules in an ultrashort intense laser field, J. Phys. B **38**, 333 (2005).

[20] F. Anis and B. D. Esry, Role of nuclear rotation in dissociation of H_2^+ in a short laser pulse, Phys. Rev. A **77**, 033416 (2008).

[21] J. McKenna, A. M. Sayler, F. Anis, B. Gaire, N. G. Johnson, E. Parke, J. J. Hua, H. Mashiko, C. M. Nakamura, E. Moon, Z. Chang, K. D. Carnes, B. D. Esry, and I. Ben-Itzhak, Enhancing High-Order Above-Threshold Dissociation of H_2^+ Beams with Few-Cycle Laser Pulses, Phys. Rev. Lett. **100**, 133001 (2008).

[22] F. Anis, T. Cackowski, and B. D. Esry, Rotational dynamics of dissociating H_2^+ in a short intense laser pulse, J. Phys. B **42**, 091001 (2009).

[23] D. Ursrey, F. Anis, and B. D. Esry, Multiphoton dissociation of HeH^+ below the $He^+(1s) + H(1s)$ threshold, Phys. Rev. A **85**, 023429 (2012).

[24] Y. Yu, S. Zeng, J. V. Hernández, Y. Wang, and B. D. Esry, Influence of the initial angular distribution on strong-field molecular dissociation, Phys. Rev. A **94**, 023423 (2016).

[25] S. Wang, J. Cai, and Y. Chen, Ionization dynamics of polar molecules in strong elliptical laser fields, Phys. Rev. A **96**, 043413 (2017).

[26] R. S. Mulliken, Intensities of electronic transitions in molecular spectra, II. Charge-transfer spectra, J. Chem. Phys. **7**, 20 (1939).

[27] A. Giusti-Suzor, X. He, O. Atabek, and F. H. Mies, Above-Threshold Dissociation of H_2^+ in Intense Laser Fields, Phys. Rev. Lett. **64**, 515 (1990).

[28] G. Jolicard and O. Atabek, Above-threshold-dissociation dynamics of H_2^+ with short intense laser pulses, Phys. Rev. A **46**, 5845 (1992).

[29] L. Yue and L. B. Madsen, Dissociation and dissociative ionization of H_2^+ using the time-dependent surface flux method, Phys. Rev. A **88**, 063420 (2013).

[30] P. Lu, J. Wang, H. Li, K. Lin, X. Gong, Q. Song, Q. Ji, W. Zhang, J. Ma, H. Li, H. Zeng, F. He, and J. Wu, High-order above-threshold dissociation of molecules, Proc. Natl. Acad. Sci. USA **115**, 2049 (2018).

[31] A. D. Bandrauk and M. L. Sink, Photodissociation in intense laser fields: Predissociation analogy, J. Chem. Phys. **74**, 1110 (1981).

[32] P. H. Bucksbaum, A. Zavriyev, H. G. Muller, and D. W. Schumacher, Softening of the H_2^+ Molecular Bond in Intense Laser Fields, Phys. Rev. Lett. **64**, 1883 (1990).

[33] A. Zavriyev, P. H. Bucksbaum, J. Squier, and F. Saline, Light-Induced Vibrational Structure in H_2^+ and D_2^+ in Intense Laser Fields, Phys. Rev. Lett. **70**, 1077 (1993).

[34] L. J. Frasinski, J. H. Posthumus, J. Plumridge, K. Codling, P. F. Taday, and A. J. Langley, Manipulation of Bond Hardening in H_2^+ by Chirping of Intense Femtosecond Laser Pulses, Phys. Rev. Lett. **83**, 3625 (1999).

[35] M. F. Kling, C. Siedschlag, A. J. Verhoef, J. I. Khan, M. Schultze, T. Uphues, Y. Ni, M. Uiberacker, M. Drescher, F. Krausz, and M. J. J. Vrakking, Control of electron localization in molecular dissociation, Science **312**, 246 (2006).

[36] A. Staudte, D. Pavičić, S. Chelkowski, D. Zeidler, M. Meckel, H. Niikura, M. Schöffler, S. Schössler, B. Ulrich, P. P. Rajeev, T. Weber, T. Jahnke, D. M. Villeneuve, A. D. Bandrauk, C. L. Cocke, P. B. Corkum, and R. Dörner, Attosecond Strobing of Two-Surface Population Dynamics in Dissociating H_2^+, Phys. Rev. Lett. **98**, 073003 (2007).

[37] M. Waitz, D. Aslitürk, N. Wechselberger, H. K. Gill, J. Rist, F. Wiegandt, C. Goihl, G. Kastirke, M. Weller, T. Bauer, D. Metz, F. P. Sturm, J. Voigtsberger, S. Zeller, F. Trinter, G. Schiwietz, T. Weber, J. B. Williams, M. S. Schöffler, L. P. H. Schmidt, T. Jahnke, and R. Dörner, Electron Localization in Dissociating H_2^+ by Retroaction of a Photoelectron Onto its Source, Phys. Rev. Lett. **116**, 043001 (2016).

[38] H. Xu, Z. Li, F. He, X. Wang, A. Atia-Tul-Noor, D. Kielpinski, R. T. Sang, and I. V. Litvinyuk, Observing electron localization in a dissociating H_2^+ molecule in real time, Nat. Commun. **8**, 15849 (2017).

[39] B. D. Esry, A. M. Sayler, P. Q. Wang, K. D. Carnes, and I. Ben-Itzhak, Above Threshold Coulomb Explosion of Molecules in Intense Laser Pulses, Phys. Rev. Lett. **97**, 013003 (2006).

[40] E. Dehghanian, A. D. Bandrauk, and G. L. Kamta, Enhanced ionization of the non-symmetric HeH^+ molecule driven by intense ultrashort laser pulses, J. Chem. Phys. **139**, 084315 (2013).

[41] B. O. Roos, P. R. Taylor, and P. E. Siegbahn, A complete active space SCF method (CASSCF) using a density matrix formulated super-CI approach, Chem. Phys. **48**, 157 (1980).

[42] F. Aquilante, J. Autschbach, R. K. Carlson, L. F. Chibotaru, M. G. Delcey, L. De Vico, I. Fdez. Galván, N. Ferré, L. M. Frutos, L. Gagliardi, M. Garavelli, A. Giussani, C. E. Hoyer, G. Li Manni, H. Lischka, D. Ma, P. Å. Malmqvist, T. Müller, A. Nenov, M. Olivucci, T. B. Pedersen, D. Peng, F. Plasser, B. Pritchard, M. Reiher, I. Rivalta, I. Schapiro, J. Segarra-Martí, M. Stenrup, D. G. Truhlar, L. Ungur, A. Valentini, S. Vancoillie, V. Veryazov, V. P. Vysotskiy, O. Weingart, F. Zapata, and R. Lindh, MOLCAS 8: New capabilities for multiconfigurational quantum chemical calculations across the periodic table, J. Comput. Chem. **37**, 506 (2016).

[43] J. Deiglmayr, M. Aymar, R. Wester, M. Weidemüller, and O. Dulieu, Calculations of static dipole polarizabilities of alkali dimers: Prospects for alignment of ultracold molecules, J. Chem. Phys. **129**, 064309 (2008).

[44] T. Fiedlschuster, J. Handt, and R. Schmidt, Floquet surface hopping: Laser-driven dissociation and ionization dynamics of H_2^+, Phys. Rev. A **93**, 053409 (2016).

[45] O. I. Tolstikhin, L. B. Madsen, and T. Morishita, Weak-field asymptotic theory of tunneling ionization in many-electron atomic and molecular systems, Phys. Rev. A **89**, 013421 (2014).

[46] L. Yue, S. Bauch, and L. B. Madsen, Electron correlation in tunneling ionization of diatomic molecules: An application of the many-electron weak-field asymptotic theory with a generalized-active-space partition scheme, Phys. Rev. A **96**, 043408 (2017).

[47] G. L. Kamta and A. D. Bandrauk, Nonsymmetric molecules driven by intense few-cycle laser pulses: Phase and orientation dependence of enhanced ionization, Phys. Rev. A **76**, 053409 (2007).

[48] J. Loreau, J. Lecointre, X. Urbain, and N. Vaeck, Rovibrational analysis of the XUV photodissociation of HeH^+ ions, Phys. Rev. A **84**, 053412 (2011).

[49] W. Ketterle, H. Figger, and H. Walther, Emission Spectra of Bound Helium Hydride, Phys. Rev. Lett. **55**, 2941 (1985).

[50] P. Wang, A. M. Sayler, K. D. Carnes, B. D. Esry, and I. Ben-Itzhak, Disentangling the volume effect through intensity-difference spectra: Application to laser-induced dissociation of H_2^+, Opt. Lett. **30**, 664 (2005).

[51] P. Wustelt, F. Oppermann, L. Yue, M. Möller, T. Stöhlker, M. Lein, S. Gräfe, G. G. Paulus, and A. M. Sayler, Heteronuclear Limit of Strong-Field Ionization: Fragmentation of HeH^+ by Intense Ultrashort Laser Pulses, Phys. Rev. Lett. **121**, 073203 (2018).

[52] O. I. Tolstikhin, H. J. Wörner, and T. Morishita, Effect of nuclear motion on tunneling ionization rates of molecules, Phys. Rev. A **87**, 041401 (2013).

[53] X. Wang, H. Xu, A. Atia-Tul-Noor, B. T. Hu, D. Kielpinski, R. T. Sang, and I. V. Litvinyuk, Isotope Effect in Tunneling Ionization of Neutral Hydrogen Molecules, Phys. Rev. Lett. **117**, 083003 (2016).